On femtosecond micromachining of HPHT single-crystal diamond with direct laser writing using tight focusing

Othman H. Y. Zalloum,* Matthew Parrish, Alexander Terekhov, and William Hofmeister

The University of Tennessee Space Institute, 411 B.H. Goethert Parkway, Tullahoma, TN, 37388, USA
**ozalloum@utsi.edu*

Abstract: We investigate the formation of diversiform micro-/nano-structures in High-Pressure High-Temperature (HPHT) synthetic single-crystal diamond by tight-focusing 200 fs regeneratively amplified Ti: Sapphire laser pulses centered at λ = 800 nm. Ablated samples of synthetic single crystal nanodiamond and their acetate replicas are analyzed using scanning electron microscopy (SEM). Using pulse energies that are significantly above the threshold for permanent change, it is shown from this work that amplified femtosecond pulses are capable of producing controlled modification of HPHT single-crystal diamond at size scales below the diffraction limit and provided negligible collateral heating and shock-wave damage. This is attributed to the low thermal losses and negligible hydrodynamic expansion of the ablated material during the femtosecond laser pulse. It is shown that low pulse energy is a key factor for the accurate and precise machining of micropattems.

OCIS codes: (350.3390) Laser materials processing; (220.4241) Nanostructure fabrication; (320.2250) Femtosecond phenomena.

References and Links

1. B. C. Stuart, M. D. Feit, A. M. Rubenchik, B. W. Shore, and M. D. Perry, "Laser-induced damage in dielectrics with nanosecond to subpicosecond pulses," Phys. Rev. Lett. **74**(12), 2248–2251 (1995).
2. B. C. Stuart, M. D. Feit, S. Herman, A. M. Rubenchik, B. W. Shore, and M. D. Perry, "Nanosecond-to-femtosecond laser-induced breakdown in dielectrics," Phys. Rev. B Condens. Matter **53**(4), 1749–1761 (1996).
3. E. Mazur, "Applications of femtosecond lasers in materials processing," in *Conference on Lasers and Electro-Optics Europe* (Munich, Germany, 2009).
4. J. Perriere, E. Millon, and E. Fogarassy, eds., *Recent Advances in Laser Processing of Materials* (Elsevier, 2006).
5. H. Misawa, and S. Juodkazis, eds., *3D Laser Microfabrication: Principles and Applications* (Wiley-VCH Verlag GmbH & Co. KGaA, Weinheim, 2006).
6. C. Phipps, ed., *Laser Ablation and its Applications* (Springer, New York, 2007).
7. B. C. Stuart, M. D. Feit, A. M. Rubenchik, B. W. Shore, and M. D. Perry, "Laser-induced damage in dielectrics with nanosecond to subpicosecond pulses," Phys. Rev. Lett. **74**(12), 2248–2251 (1995).
8. A. P. Joglekar, H. Liu, G. J. Spooner, E. Meyhofer, G. Mourou, and A. J. Hunt, "A study of the deterministic character of optical damage by femtosecond laser pulses and applications to nanomachining," Appl. Phys. B **77**(1), 25–30 (2003).
9. A. P. Joglekar, H. H. Liu, E. Meyhöfer, G. Mourou, and A. J. Hunt, "Optics at critical intensity: applications to nanomorphing," Proc. Natl. Acad. Sci. U.S.A. **101**(16), 5856–5861 (2004).
10. C. B. Schaffer, N. Nishimura, E. N. Glezer, A. M. T. Kim, and E. Mazur, "Dynamics of femtosecond laser-induced breakdown in water from femtoseconds to microseconds," Opt. Express **10**(3), 196–203 (2002).
11. M. Sakakura, and M. Terazima, "Initial temporal and spatial changes of the refractive index induced by focused femtosecond pulsed laser irradiation inside a glass," Phys. Rev. B **71**(2), 024113 (2005).
12. M. Sakakura, M. Terazima, Y. Shimotsuma, K. Miura, and K. Hirao, "Observation of pressure wave generated by focusing a femtosecond laser pulse inside a glass," Opt. Express **15**(9), 5674–5686 (2007).
13. B. Qian, J. Song, G. P. Dong, L. B. Su, B. Zhu, X. F. Liu, S. Z. Sun, Q. Zhang, and J. R. Qiu, "Formation and partial recovery of optically induced local dislocations inside CaF2 single crystal," Opt. Express **17**(10), 8552–8557 (2009).
14. M. Sakakura, M. Terazima, Y. Shimotsuma, K. Miura, and K. Hirao, "Heating and rapid cooling of bulk glass after photoexcitation by a focused femtosecond laser pulse," Opt. Express **15**(25), 16800–16807 (2007).

#126118 - $15.00 USD Received 29 Mar 2010; revised 28 May 2010; accepted 29 May 2010; published 3 Jun 2010

15. C. W. Carr, H. B. Radousky, A. M. Rubenchik, M. D. Feit, and S. G. Demos, "Localized dynamics during laser-induced damage in optical materials," Phys. Rev. Lett. **92**(8), 087401 (2004).
16. N. Bloembergen, "Laser-induced electric breakdown in solids," IEEE J. Sel. Top. Quantum Electron. **10**(3), 375–386 (1974).
17. S. K. Sundaram, and E. Mazur, "Inducing and probing non-thermal transitions in semiconductors using femtosecond laser pulses," Nat. Mater. **1**(4), 217–224 (2002).
18. R. R. Gattass, and E. Mazur, "Femtosecond laser micromachining in transparent materials," Nat. Photonics **2**(4), 219–225 (2008).
19. B. N. Chichkov, C. Momma, S. Nolte, F. Alvensleben, and A. Tünnermann, "Femtosecond, picosecond and nanosecond laser ablation of solids," Appl. Phys., A Mater. Sci. Process. **63**(2), 109–115 (1996).
20. X. Liu, D. Du, and G. Mourou, "Laser ablation and micromachining with ultrashort laser pulses," IEEE J. Quantum Electron. **33**(10), 1706–1716 (1997).
21. C. L. Arnold, A. Heisterkamp, W. Ertmer, and H. Lubatschowski, "Computational model for nonlinear plasma formation in high NA micromachining of transparent materials and biological cells," Opt. Express **15**(16), 10303–10317 (2007).
22. E. N. Glezer, M. Milosavljevic, L. Huang, R. J. Finlay, T. H. Her, J. P. Callan, and E. Mazur, "Three-dimensional optical storage inside transparent materials," Opt. Lett. **21**(24), 2023–2025 (1996).
23. D. Ashkenasi, M. Lorenz, R. Stoian, and A. Rosenfeld, "Surface damage threshold and structuring of dielectrics using femtosecond laser pulses: the role of incubation," Appl. Surf. Sci. **150**(1-4), 101–106 (1999).
24. F. Ahmed, and M. S. Lee, "Micromachining of Grooves for Cutting Fused Silica Plates with Femtosecond Laser Pulses," in *in Conference on Lasers and Electro-Optics/Pacific Rim 2007, (Optical Society of America, 2007), paper TuB2_3.*
25. T. V. Kononenko, M. Meier, M. S. Komlenok, S. M. Pimenov, V. Romano, V. P. Pashinin, and V. I. Konov, ""Microstructuring of diamond bulk by IR femtosecond laser pulses," Appl. Phys," Adv. Mater. **90**, 645–651 (2008).
26. M. Shinoda, K. Saito, T. Kondo, A. Nakaoki, M. Furuki, M. Takeda, M. Yamamoto, T. J. Schaich, B. M. Van Oerle, H. P. Godfried, P. A. C. Kriele, E. P. Houwman, W. H. M. Nelissen, G. J. Pels, and P. G. M. Spaaij, "High-density near-field readout using diamond solid immersion lens," Jpn. J. Appl. Phys. **45**(No. 2B), 1311–1313 (2006).
27. D. Ramanathan, and P. A. Molian, "Micro- and sub-micromachining of type IIa single crystal diamond using a Ti: Sapphire femtosecond laser," J. Manuf. Sci. Eng. **124**(2), 389–396 (2002).
28. M. Takesada, E. Vanagas, D. Tuzhilin, I. Kudryashov, S. Suruga, H. Murakami, N. Sarukura, K. Matsuda, S. Mononobe, T. Saiki, M. Yoshimoto, and S. Y. Koshihara, "Micro-character printing on a diamond plate by femtosecond infrared optical pulses," Jpn. J. Appl. Phys. **42**(Part 1, No. 7A), 4613–4616 (2003).
29. P. Olivero, S. Rubanov, P. Reichart, B. C. Gibson, S. T. Huntington, J. R. Rabeau, A. D. Greentree, J. Salzman, D. Moore, D. N. Jamieson, and S. Prawer, "Characterization of three-dimensional microstructures in single-crystal diamond," Diamond Related Materials **15**(10), 1614–1621 (2006).
30. J. L. Davidson, W. P. Kang, Y. Gurbuz, K. C. Holmes, L. G. Davis, A. Wisitsora-at, D. V. Kerns, R. L. Eidson, and T. Henderson, "Diamond as an active sensor material," Diamond Related Materials **8**(8-9), 1741–1747 (1999).
31. W. P. Kang, T. S. Fisher, and J. L. Davidson, "Diamond microemitters - The new frontier of electron field emissions and beyond," New Diamond Front. Carbon Technol. **11**, 129–146 (2001).
32. *http://www.diamondedgeco.com/11533.html*, "High Quality Diamond Knives," (Diamond Edge Company, 2010), Accessed 05/24/2010.
33. D. Gómez, I. Goenaga, I. Lizuain, and M. Ozaita, "Femtosecond laser ablation for microfluidics," Opt. Eng. **44**(5), 051105 (2005).
34. C. Mauclair, A. Mermillod-Blondin, N. Huot, E. Audouard, and R. Stoian, "Ultrafast laser writing of homogeneous longitudinal waveguides in glasses using dynamic wavefront correction," Opt. Express **16**(8), 5481–5492 (2008).
35. K. Subramanian, W. P. Kang, J. L. Davidson, and M. Howell, "Nanodiamond lateral field emitter devices on thick insulator substrates for reliable high power applications," Diamond Related Materials **17**(4-5), 786–789 (2008).
36. Y. F. Tzeng, K. H. Liu, Y. C. Lee, S. J. Lin, I. N. Lin, C. Y. Lee, and H. T. Chiu, "Fabrication of an ultra-nanocrystalline diamond-coated silicon wire array with enhanced field-emission performance," Nanotechnology **18**(43), 435703 (2007).
37. Y. L. Liou, J. C. Liou, J. H. Huang, N. H. Tai, and I. N. Lin, "Fabrication and field emission properties of ultra-nanocrystalline diamond lateral emitters," Diamond Related Materials **17**(4-5), 776–781 (2008).
38. T. N. Kim, K. Campbell, A. Groisman, D. Kleinfeld, and C. B. Schaffer, "Femtosecond laser-drilled capillary integrated into a microfluidic device," Appl. Phys. Lett. **86**, 201106 (2005).
39. T. S. Fisher, "Influence of nanoscale geometry on the thermodynamics of electron field emission," Appl. Phys. Lett. **79**(22), 3699–3701 (2001).
40. T. V. Kononenko, M. Meier, M. S. Komlenok, S. M. Pimenov, V. Romano, V. P. Pashinin, and V. I. Konov, ""Microstructuring of diamond bulk by IR femtosecond laser pulses," Appl. Phys," Adv. Mater. **90**, 645–651 (2008).
41. M. Shinoda, R. R. Gattass, and E. Mazur, "Femtosecond laser-induced formation of nanometer-width grooves on synthetic single-crystal diamond surfaces," J. Appl. Phys. **105**(5), 053102 (2009).
42. G. Dumitru, V. Romano, H. P. Weber, M. Sentis, and W. Marine, "Femtosecond ablation of ultrahard materials," Appl. Phys., A Mater. Sci. Process. **74**(6), 729–739 (2002).

#126118 - $15.00 USD Received 29 Mar 2010; revised 28 May 2010; accepted 29 May 2010; published 3 Jun 2010

43. K. Subramanian, W. P. Kang, J. L. Davidson, W. H. Hofmeister, B. K. Choi, and M. Howell, "Nanodiamond planar lateral field emission diode," Diamond Related Materials **14**(11-12), 2099–2104 (2005).
44. M. Groenendijk, and J. Meijer, "Microstructuring using femtosecond pulsed laser ablation," J. Laser Appl. **18**(3), 227–235 (2006).
45. D. C. Emmony, R. P. Howson, and L. J. Willis, "Laser Mirror Damage in Germanium at 10.6 μm," Appl. Phys. Lett. **23**(11), 598–600 (1973).
46. Z. Guosheng, P. Fauchet, and A. Siegman, "Growth of Spontaneous Periodic Surface-Structures on Solids During Laser Illumination," Phys. Rev. B **26**(10), 5366–5381 (1982).
47. A. J. Pedraza, Y. F. Guan, J. D. Fowlkes, and D. A. Smith, "Nanostructures produced by ultraviolet laser irradiation of silicon. I. Rippled structures," J. Vac. Sci. Technol. B **22**(6), 2823–2835 (2004).
48. R. Le Harzic, H. Schuck, D. Sauer, T. Anhut, I. Riemann, and K. König, "Sub-100 nm nanostructuring of silicon by ultrashort laser pulses," Opt. Express **13**(17), 6651–6656 (2005).

1. Introduction

A femtosecond pulse of sufficient energy when focused inside a material will optically breakdown [1,2]. Optical breakdown can be understood in terms of creation of seed electrons by multiphoton ionization [3–6] or tunneling ionization [7,8] followed by avalanche ionization in which the seed electrons are driven by the laser field and then cause secondary collisional ionization [9]. Over a picosecond timescale, part of the optical energy absorbed by the electrons is transferred to the lattice. Usually a pressure or a shockwave occurs and separates from the hot focal volume within a couple of nanoseconds [10–13]. The thermal energy diffuses out of the focal volume on a microsecond timescale [14,15]. At a sufficiently high energy, these processes cause melting or non-thermal ionic motion and leave behind permanent structural changes. Thus, a femtosecond laser pulse ends before the electrons thermally excite any ions. Heat diffusion outside the focal area is minimized, increasing the precision of the method. Ablation takes place when the density of free conduction band electrons reaches a critical density. This happens above a certain laser fluence threshold at which point the electrostatic forces are high enough to breakdown the material and to eject the ionized nuclei. When the density of excited electrons is sufficiently high, the electrons behave as a plasma with a natural frequency that is resonant with the laser leading to reflection and absorption of the remaining pulse energy [1,16]. The repeatability and tight confinement of the nonlinear excitation enable the use the femtosecond-laser-induced damage for practical purpose [17–20].

Recent applications of ultrashort pulses in transparent materials have evolved towards tight focusing at high numerical aperture to reduce pulse energy, enhance precision, and limit nonlinear side effects [21,22]. For a homogeneous plane wavefront incident on a diffraction-limited optical system having radial symmetry, the radius of the first Airy disk can be estimated as $0.61\ \lambda/NA$, where λ is the laser wavelength and NA is the numerical aperture of the focusing objective. Using ultrashort laser pulses, there is a further possibility to overcome the diffraction limit on transparent materials. The geometry of the final structure in femtosecond single shot ablation can be influenced by the pulse intensity and the numerical aperture. The latter determines the width of the focal volume and therefore the resulting feature size. For NA larger than 0.6, the micromachined features are almost spherically symmetric; below this value, the resulting structures become larger and asymmetric. Changing the spatial profile and divergence of the input beam prior to focusing, such that the focal-spot profile is closer to a symmetric circular cross-section, can mitigate the asymmetry [20,21]. The dependence of the spherical symmetry on the NA is usually due to the fact that the axial focus size is much larger than the transverse size, except for tight focusing conditions. This is mostly relevant for the structuring in the bulk of transparent materials as used, for instance, in waveguide writing in glass.

The laser fluence is a fundamental parameter in laser material processing. As laser fluence increases, the ablation width and depth per pulse also increases. The ablation threshold is expected to decrease for increasing number of overlapping pulses due to material dependent "incubation effect" [23]. Previous publications on femtosecond modifications to dielectrics showed that the depth of a single pass groove almost linearly depends on the energy of pulses while decreases exponentially as the translation speed increases. The ablation depth

#126118 - $15.00 USD Received 29 Mar 2010; revised 28 May 2010; accepted 29 May 2010; published 3 Jun 2010

exponentially increases as the effective number of pulses incident on the sample increases [24].

Diamond is the ultimate material in terms of hardness, elastic modulus, thermal conductivity, electrical resistivity and refractive index [24]. Synthetic diamond is much cheaper and more accessible than the natural diamond, so it is more attractive for possible industrial applications [25–29]. Synthetic diamond has tremendous potential as an advanced, high temperature electronic material, and considerable research has been conducted to try to capture the benefits of this material system in engineering applications such as high temperature, pressure and chemical sensors [30] and most notably, as electron emitters [31].

Femtosecond machining of HPHT diamond has many interesting aspects. It avoids the tool wear experienced by traditional machining techniques, while the femtosecond pulse delivers extreme peak irradiance with minimal thermal effects. The HPHT diamond crystals are typically a few mm in size, which are extremely useful as hard-wearing edges on cutting tools, drill-bits and scalpels for surgery [32] and the femtosecond laser processing of this material could lead to many novel technologies. Femtosecond machining of HPHT diamond may also find applications in the creation of passive microfluidic devices [33], waveguides [34], and electron emitting devices for high speed or high power electronics [35–37]. In some cases, one can create complex structures and patterns that are not possible with other techniques [38].

In this paper, we investigate the femtosecond micromachining of diversiform structures in HPHT synthetic single-crystal diamond using a newly developed integrated scanning microscope for femtosecond machining and Raman spectroscopy ruling out possible imprecisions coming from the use of the two independent techniques. Our motivation for the choice of the various shapes and configurations stems mainly from our interest to investigate the edge quality of the machined surfaces. Microscale channels, pointed structures and more complex designs were ablated. These shapes can be important elements in microfluidic devices, electron emitters and 3D applications of femtosecond machining, respectively. Microfluidic devices usually include microscale channels, bends, joints and reservoirs. Moreover, a basic premise of diamond emitters is the use of pointed structures; nanostructured emission tips (cathode). A very tight radius of curvature at the emission tip is known to enhance electron emission by reducing the tunneling barrier to electron emission [39]. Investigation of the ablated edge quality and the size of feature of the machined structures are important to understand to give insight for the development of future fully-integrated assemblies.

We show that by using pulse energies significantly above the threshold for permanent change, one can micromachine efficiently with good geometry and quality due to the minimal thermal effects and negligible hydrodynamic expansion of the ablated material during the femtosecond laser pulse. We present surface structuring of HPHT synthetic single crystal diamond by various pulse fluences and numbers of femtosecond pulses with particular attention paid to the effects on the feature size and the edge quality of a feature. These effects are important to consider when comparing the results with different experiments and theoretical models in the literature, since the optical properties and chemical composition of the target and atmosphere are not the only factors which can influence the final morphology.

2. Materials and methods

Figure 1(a) shows amplified femtosecond pulses are generated by a system consisting of Tsunami oscillator (Spectra Physics-model 3941) seeding a RegA 9000 (Coherent, Inc.) regenerative amplifier, both of which are pumped with CW green solid-state Verdi-18 laser (Coherent, Inc.). The amplified 4μJ, 800 nm femtosecond pulses are directed to a newly developed scanning microscope workstation which combines Raman spectroscopy and femtosecond ablation as shown in Fig. 1(b). The scanning microscope focuses femtosecond pulses onto samples placed on mobile stages under computer control. Irradiation was controlled by a fast computer driven mechanical shutter based on an electro-magnetic actuator (Uniblitz LS6ZM2, Vincent Associates, Rochester, NY) in the laser path controlled by a

#126118 - $15.00 USD Received 29 Mar 2010; revised 28 May 2010; accepted 29 May 2010; published 3 Jun 2010

shutter driver (Uniblitz VMM-D3, Vincent Associates). This shutter has an opening diameter of 6 mm and a typical transfer time on opening (closing) of 0.7 ms (0.8 ms).

A central PC controls digital delay and pulse generation for pulse type single shot or high repetition rates, shutter control for ablation duration, and nanostage and motion control units for positioning features on the sample. The multimode fiber is coupled to a research grade spectrometer (Ocean Optics Inc., model QE65000) which is equipped with a thermoelectric (TE)-cooled and a two dimensional back-illuminated charged coupled device (CCD) detector. The spectrometer via a built-in 16 bit analog-to-digital converter (A/D) and a PC are used to gather and process the Raman signal.

Two iris diaphragms (IDs) were used to define the femtosecond beam. At a repetition rate of R = 250 kHz, if the average power is 1.0 W, the output pulse energy $E = P_{av}/R = 4$ μJ. This is where the RegA 9000 is routinely operated. Average beam power is controlled by neutral density filter wheels and was measured at the entrance pupil of the objective using a power meter (Coherent, Inc). In the scanning microscope, the sample is mounted on a piezoelectric nanostage (Mad City Labs, Inc.) which is positioned on a large range of XY motion microstage (McBain, Inc. precision stages and Compumotor, Inc. stepper motors with National Instruments motor drivers) to cover large areas of the sample. The stage is moved in a pre-programmed *x, y* pattern under LabVIEW control. The scanning microscope includes a digital imaging capability valuable to capture digital images for femtosecond machining for educational, research or archival purposes. It is also a precise focusing aid and is important for proper sample location and to monitor the progress of the operation. The camera is directly controlled by the computer which is equipped with a Camera Link frame grabber (National Instruments PCI-1426) to acquire images.

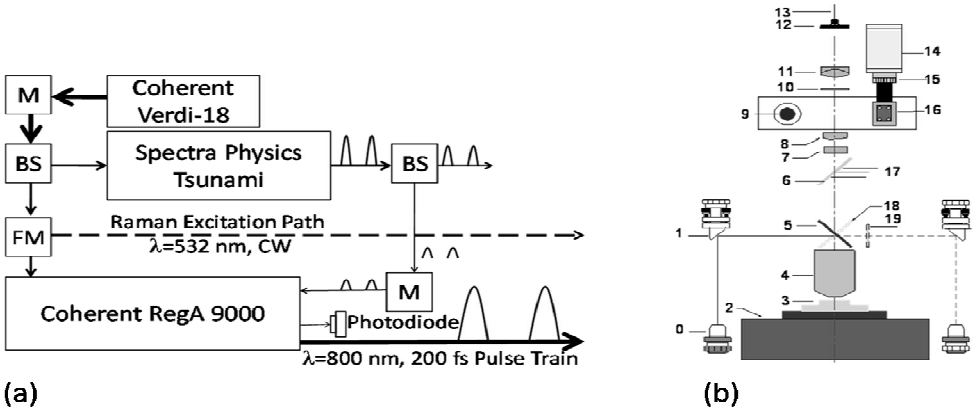

Fig. 1. (a), The amplified femtosecond pulse generation block producing the 4μJ, 800nm, 200 fs pulses. The amplified femtosecond pulses are generated with a system consisting of Tsunami oscillator (Spectra Physics-model 394) seeding a RegA 9000 (Coherent, Inc.) regenerative amplifier, both of which are pumped with CW 532 nm solid-state Verdi-18 laser (Coherent, Inc.). The Raman excitation pump is derived from the Verdi-18 solid state laser nm and is delivered to the microscope using a periscope assembly. Also shown is the "oscillator only' output. The photodiode is connected to an oscilloscope to display the repetition rate and the status of the amplified femtosecond pulse train, M: 45 ° mirror, BS beam splitter, FM; 45° flip mirror, and (b), the optical system model that represents the fabrication workstation and the integrated Raman microscope. The periscope assembly redirects and changes the elevation of a beam, and consists of a pair of 45° mirrors (0) and (1) with lockable adjustment knobs to provide 360° of rotation of the incoming light. The upper housing also provides fine control, which can be used to compensate for angular deviations of the input beam, (2) is a x-y microstage, (3), xyz nanostage, (4) infinity corrected microscope objective, (5) 800 nm dichroic filter mirror, (6) half-mirror, (7 and 8), tube lens, (9) eye piece, (10) long wave pass Raman edge filter, (11) focusing lens, (12) fiber optic endplate, (13) multimode fiber, (14) 12 bit digital camera, (15) 9 mm computer TV lens, (16) 45° mirror, (17) white light illumination produced from a reflected light vertical illuminator, (18) 532 nm dichroic filter mirror, (19) 532 nm narrow bandpass filter.

#126118 - $15.00 USD Received 29 Mar 2010; revised 28 May 2010; accepted 29 May 2010; published 3 Jun 2010

The Raman excitation pump is derived from the Verdi-18 solid state laser operating at 532 nm and is delivered to the microscope using the right PA as shown in Fig. 1(b). The 532 nm laser beam then passes through a narrow bandpass filter. The collimated laser beam is reflected by a dichroic filter mirror and focused onto the sample with an infinity corrected microscope objective. The incident and backscattered light fills the objective lens pupil. The Raman dichroic filter mirror reflects the 532 nm laser line incident at 45° while transmitting longer Raman-shifted wavelengths. The Raman-backscattered light is then collected by the same microscope objective and brought to focus onto the core of a multimode optical fiber after being passed through a long wave pass Raman edge filter.

Unless otherwise specified, the amplified 800 nm femtosecond pulse was incident normal to the sample surface and focused by a 100X microscope objective with a NA of 0.9. With these parameters, the theoretical diffraction limited beam diameter at $1/e^2$ level (13.5% of the peak value), $1.22\lambda/NA$, is approximately 1.1 μm. An imaging technique was used to measure the spot size, which confirmed a spot size diameter of approximately 1 μm. During ablation, the microstage is stationary and the nanostage scans at 11 μm/s to create the micropatterns.

Laser machining was conducted at a controlled constant room temperature and pressure in a Class-1000 clean room on a vibration isolation table. The externally triggered shutter controlled the 3 ms ablation time used in this work for the high repetition rates experiments. For the single pulse experiments, the laser system is adjusted to external triggering using the electronic control unit of RegA 9000 and under LabVIEW control, TTL pulses are directed from the real time computer to the electronic control system of RegA 9000 via a TTL pulse/delay generator (DG535, Stanford Research Systems, Inc.). The electronic control system of RegA 9000 displays the systems operating conditions and provides complete timing control of pulse injection, dumping and gain-switching.

All samples were cleaned in an ultrasonic bath with acetone, methanol, and de-ionized water, and dried with nitrogen before the experiments. The diamond samples were also cleaned after ablation for 30 minutes in acetone followed by 30 minutes in methanol in the ultrasonic cleaner in order to remove any debris from the ablation process. The samples were then sputter coated with a thin layer of gold to ensure good conductivity when viewing the samples by the scanning electron microscope (SEM).

To estimate the structure depth for laser machining we used cellulose acetate films from Electron Microscope Sciences, Inc. for sample replication. This cellulose acetate material is 35μm thick and soluble in acetone. For sample preparation, we cut out a piece of the replica material of a size suitable to cover the area to be replicated. A few drops of acetone are placed on the specimen surface and the replica film was applied immediately. Surface tension forces pull the film down against the specimen; no pressure is required. The film is left to dry for 30 minutes and gently lifted with tweezers once it has hardened. It is then mounted on a SEM sample holder using carbon tape and then sputter coated with thin layer of gold for examination in the SEM.

3. Results and discussion

Figure 2 illustrates ablation of a saw-tooth structure on synthetic single crystal nanodiamond surface created from a design containing multiple triangles, each measuring 40 μm in height and 20 μm at the base. The structure contains three triangular wedges that taper down to a blunt tip within a few micrometers of the opposite surface.

Diamond has an indirect bandgap, E_g, of 5.49 eV. The direct bandgap is approximately 7.3 eV [40]. The optical absorption edge is 235 nm [26,41]. The diamond sample had an area of 1.78 mm^2, and 0.17 mm thickness. The diamond sample in Fig. 2 was irradiated 3 times at the initial working distance of the microscope objective with a pulse train of 200-fs laser pulses at a rate of 250 kHz with a pulse energy of 420 nJ. The 250 kHz repetition rate using the shutter ablation time of 3 ms corresponds to 750 overlapping pulses. The estimated height of the replica in Fig. 2(b) is 5.6 μm. Achievable structure sizes vary in the range from several tens of microns down to submicron dimensions, depending particularly on the pulse energy and

#126118 - $15.00 USD Received 29 Mar 2010; revised 28 May 2010; accepted 29 May 2010; published 3 Jun 2010

focusing strategy. For example, by scanning a surface using femtosecond lasers or oscillators delivering just nanojoules of energy per pulse, precise triangular shapes may be ablated.

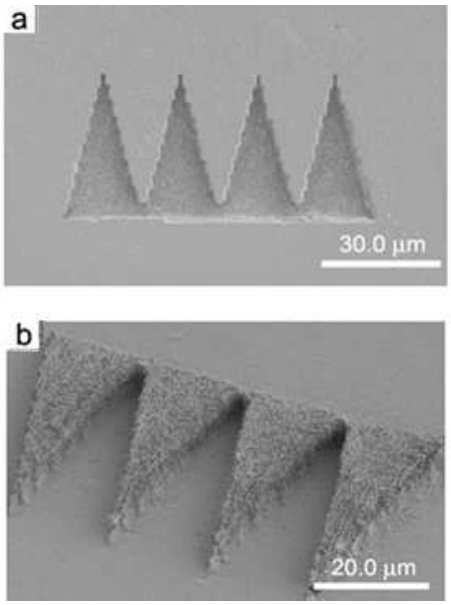

Fig. 2. Illustrates ablation of saw-tooth structures single crystal diamond surfaces. In (b) gold coated extraction replicas of the saw-tooth patterns from (a) is shown with 45 degree tilt.

The jagged boundary lines shown in Fig. 2(a) are due to the resolution used to test and build these shapes. The original programming resolution correlating to these shapes was set to one increment in test space equal to one micron in actual space. Much smoother boundary lines can be created using smaller increments. The shape exhibited in Fig. 2 was analyzed for feature variation with a change in laser pulse energies as shown in Fig. 3.

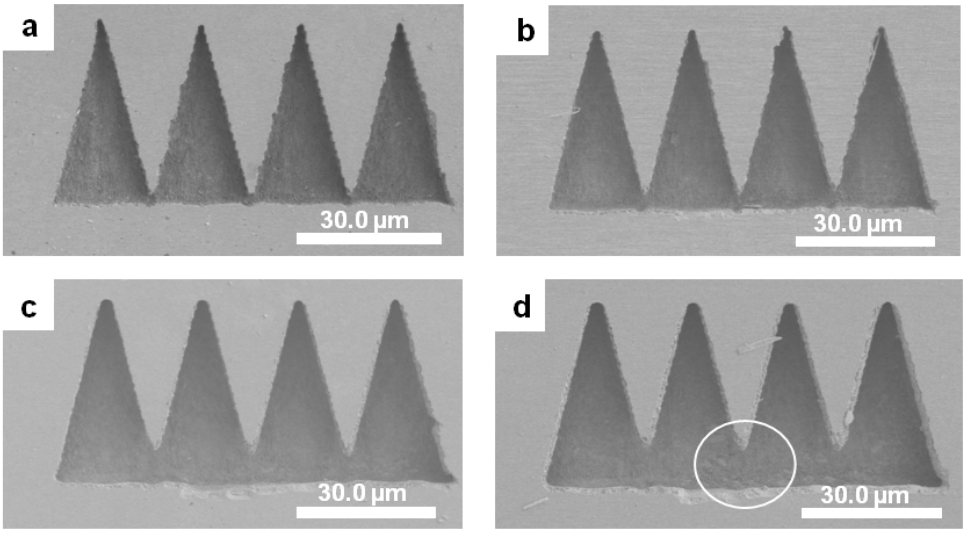

Fig. 3. Illustrates ablation of saw-tooth structures on single crystal diamond surfaces. The pulse energies are (a) 0.42 µJ, (b) 0.84 µJ, (c) 1.68 µJ, and (d) 2.52 µJ. The magnified image of the gap between two unablated sections of the shape in (d) is shown Fig. 4.

#126118 - $15.00 USD Received 29 Mar 2010; revised 28 May 2010; accepted 29 May 2010; published 3 Jun 2010

For this particular HPHT diamond, we did not notice surface structuring by SEM below energy threshold of approximately 75 nJ. This corresponds to a laser fluence of 9.6 Jcm^{-2} using a spot size diameter of 1 μm. In Fig. 3, the laser energy levels were adjusted between 420 and 2520 nJ. The actual fluence corresponding to these values ranges from about 54 to 321 Jcm^{-2}. Going significantly above the threshold is useful for applications that require high depth internal to the material and for the creation of high aspect ratio features. It is also useful to investigate the presence of collateral heating and shock-wave damage and hydrodynamic expansion of the ablated material. Previous studies with diamond materials show significant variation in bulk damage threshold from type to type. For example, Dumitru et al. [42] reported a damage threshold value of 0.40 Jcm^{-2} and an ablation threshold of approximately 1.6 Jcm^{-2}, while the damage threshold for the diamond reported by Ramanathan et al. [27] using 200-fs pulses is approximately 4 Jcm^{-2}. Defect sites in the form of point defects or impurities are likely to lower the threshold for surface ablation and enlarge the thin energy space for periodic structure formation in diamond materials.

Figure 4 is a magnified image of the gap between two unablated sections of the above shape. This figure shows two sets of lines representing the two measurements of the gap length taken for the analysis. The first measurement (s-s) is the distance between the two unablated surfaces forming the gap. The second measurement (e-e) is the minimum distance between the partially ablated bulk on either side of the gap. Figure 5 shows the results of these two measurements across a range of pulse energies. The surface-surface measurement is longer than the edge-edge measurement for every measured average power, and hence for every calculated pulse energy. This figure shows that the actual results of ablation deviate more from the shape design with increasing energy and at an almost linear rate. For the energy levels considered in this study (420-2520 nJ), we find that the lower energy offers a better chance for the accurate and precise machining of micropatterns on the surface of single crystal diamond. On the other hand, the high pulse energies are capable of producing controlled modification of HPHT single-crystal diamond and provided negligible collateral heating and shock-wave damage. This is attributed to the low thermal losses and negligible hydrodynamic expansion of the ablated material during the femtosecond laser pulse.

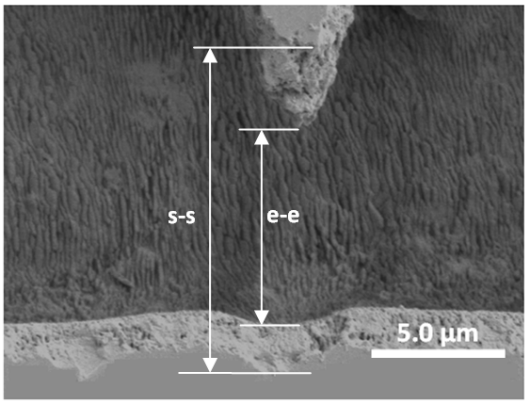

Fig. 4. Magnified image of the gap between two unablated sections of the shape in Fig. 3(d). The gap distance. (s-s) is surface- surface gap distance and (e-e) is edge-edge gap distance.

It is instructive to compare our pattern in Fig. 4 to an actual field emitter. In practice, nanodiamond planar lateral field emitters may consist of a patterned nanodiamond anode and cathode on a silicon layer; all on a SiO_2 layer on the silicon substrate with a physical anode-cathode separation as small as 2 μm, which can enable the lateral device to operate at low voltages. Very small anode–cathode spacing and versatile diamond emitter configurations have been achieved [43] using photolithography and reactive ion etching (RIE) to form such structures.

#126118 - $15.00 USD Received 29 Mar 2010; revised 28 May 2010; accepted 29 May 2010; published 3 Jun 2010

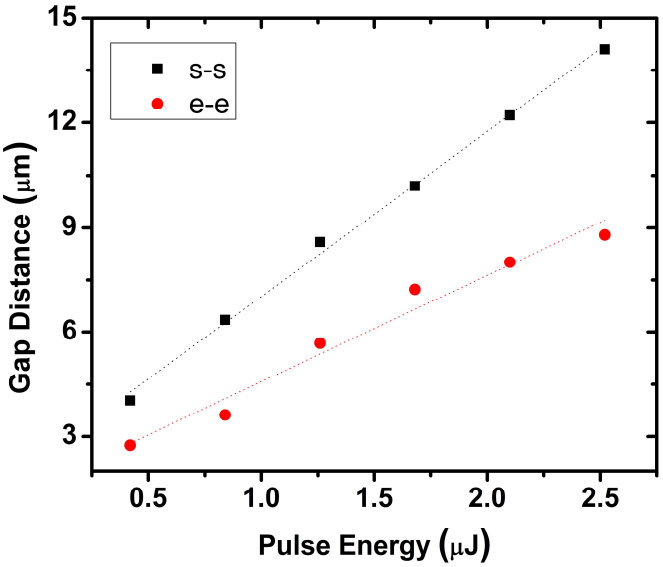

Fig. 5. Measurements of the gap distance versus laser pulse energy (μJ) at a repetition rate of 250 kHz.

To investigate whether or not the slope angle improves at lower energy, we have overlapped and slightly shifted the triangular patterns in Fig. 3(b) and 3(d) as shown in Fig. 6. It appears that the slopes of the two triangular patterns remain parallel indicating that the slope angle does not change or improve at lower energy. In addition to our earlier observations, it is noted that with higher energy the tip of the triangular patterns become more round and deviate more from the original design.

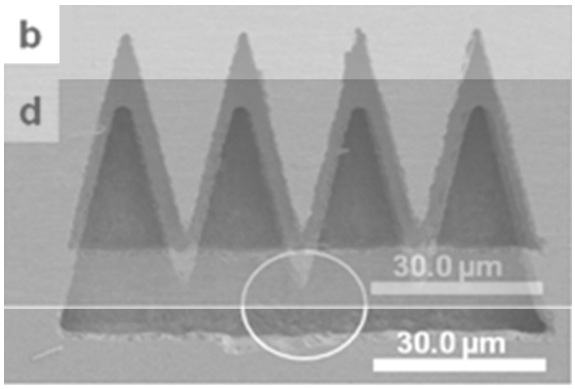

Fig. 6. Overlapped and slightly shifted (for clarity) images of the triangular patterns in Fig. 3(b) (ablated at pulse energy of 0.84μJ) and 3(d) (ablated at pulse energy of 2.52 μJ).

#126118 - $15.00 USD Received 29 Mar 2010; revised 28 May 2010; accepted 29 May 2010; published 3 Jun 2010

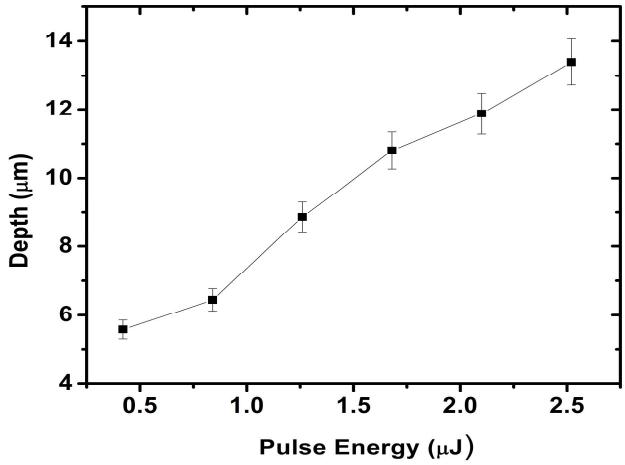

Fig. 7. Dependence of feature depth on pulse energy for the shapes in Fig. 3.

Figure 7 shows the dependence of feature depth on laser pulse energy for the shapes in Fig. 3 as estimated by acetate replication which provides a fast, nondestructive, and inexpensive technique to obtain information about sub-micron structures on and below the sample surface. The SEM stage tilt (45 degrees) has been taken into account. Overall; the increase in feature depth with laser pulse energy varies almost linearly.

We also formed periodic linear grooves in synthetic single-crystal diamond with femtosecond pulses at 800 nm as shown in Fig. 8. The grooves are obtained after irradiating the synthetic single-crystal diamond surface with a single pass of a pulse train of 200-fs laser pulses at a rate of 250 KHz using pulse energy of 1.2 μJ with a shutter open time of 3 ms at each point. The grooves can be extended to millimeter length by translating the sample under the laser beam. The step size in machining of the grooves was 0.25 μm and the horizontal line spacing in the original programming of this shape was 4 μm.

The resulting width of the periodic linear grooves near the bottom of the tracks is 0.7 ± 0.1 μm which is smaller than the theoretical diffraction-limited spot size. Table 1 summarizes descriptive statistics on measured groove widths below the upper edge of the shape. It is seen that the diffraction limit can be overcome and in this case, only the central part of the beam modifies the material resulting in subwavelength structures.

Table 1. Descriptive statistics on measured groove widths near the bottom of the tracks

Mean	Standard Deviation	Minimum	Median	Maximum
0.7 μm	0.1 μm	0.5 μm	0.7 μm	0.8 μm

From the gold coated extraction replica shown in Fig. 8(b), the groove depth is approximately 2 μm and can be controlled by varying the laser output energy, repetition rate and number of the femtosecond laser pulses. When making shapes or two-dimensional arrays of holes, the translation stage was programmed to move in a back and forth pattern at predefined intervals. During this motion the laser polarization was in the plane of the translation stage and perpendicular to the translation direction. If the first column of the grid is scanned along the *y* axis from forth to back, then when the edge of the shape is reached, the translation stage is moved to the next column by moving along the laser polarization (*x* axis). The second column of the shape is also scanned from forth to back. This column by column process continues until the entire shape or array of holes has been formed.

#126118 - $15.00 USD Received 29 Mar 2010; revised 28 May 2010; accepted 29 May 2010; published 3 Jun 2010

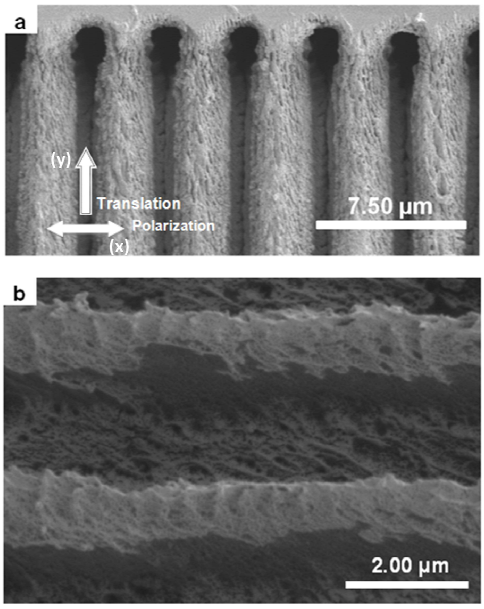

Fig. 8. SEM image of the grooves obtained after irradiating the synthetic single-crystal diamond surface with a pulse train of 200-fs laser pulses at a rate of 250 kHz using a pulse energy of 1.2 µJ. The laser polarization is oriented horizontally perpendicular to the translation direction. In (b) gold coated extraction replica of the grooves patterns from (a) is shown with 45 degree tilt.

Figure 9 shows SEM image of a star shape obtained after irradiating the synthetic single-crystal diamond surface with a pulse train of 200-fs laser pulses at a rate of 250 kHz using a pulse energy of 1.4µJ. In this regime, the result shows neither expelled resolidified liquid material at the edges of the structures nor significant formation of debris on the target surface. No evident cracks in the surrounding material are observed which indicates the absence of high ablation pressure.

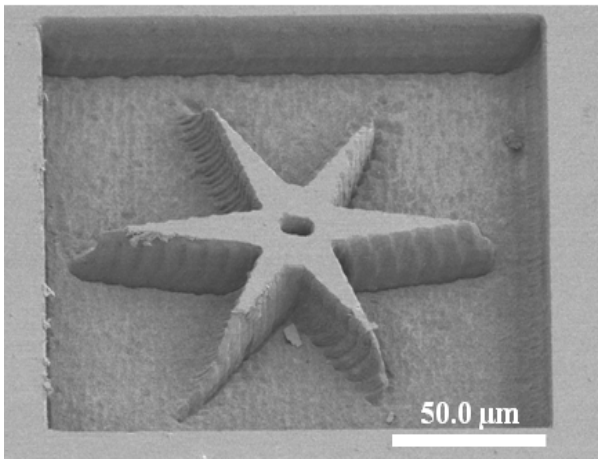

Fig. 9. SEM image of a star structure machined on the surface of the synthetic single crystal diamond by a pulse train of 200-fs laser pulses at a rate of 250 kHz using a pulse energy of 1.4 µJ.

It is interesting to note that the ablation process induced nanoscale surface morphologies in the irradiated areas of synthetic single crystal diamond as shown in Fig. 10. The periodic pattern, often referred to as laser-induced periodic structure (LIPPS), can be understood as a

#126118 - $15.00 USD Received 29 Mar 2010; revised 28 May 2010; accepted 29 May 2010; published 3 Jun 2010

very general phenomenon as it is observed on many different materials [44]. In Fig. 10, the periodic structures were formed after laser irradiation with pulses of 200 fs duration, centered at 800 nm with a pulse energy of 840 nJ. In Fig. 10(a), the sample was irradiated with a single pulse at each spot (N = 1 pulse). In Fig. 10(b), the sample was irradiated at a repetition rate of 250 kHz using a shutter open time of 3 ms, corresponding to N = 750 pulses. In both cases the machining step size was 0.25 μm and a 100X focusing objective with a NA of 0.9 was used, and the laser polarization was oriented horizontally perpendicular to the translation direction. A widely accepted model to explain these features assumes an inhomogeneous energy input across the ablated spot resulting from interference of the incident beam with microscopic fields scattered by surface roughness [45–47]. The period and orientation of these surface ripples, mainly depend on the angle of incidence, polarization, frequency, and energy of the laser beam [4,48].

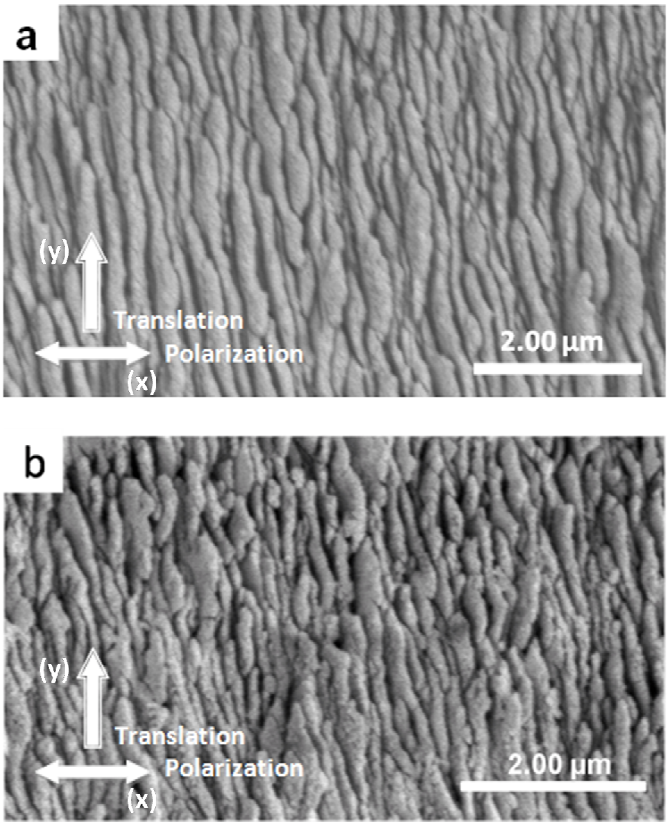

Fig. 10. (a) SEM image of periodic structures formed after laser irradiation with single pulses irradiated at each spot, and (b) the sample was irradiated at a repetition rate of 250 kHz using a shutter open time of 3 ms, corresponding to N = 750 pulses. In both cases, the step size was 0.25 μm and a 100X focusing objective with a NA of 0.9 was used to focus the 200fs pulses, centered at 800 nm with energy of 840 nJ/pulse. The laser polarization was oriented horizontally perpendicular to the translation direction.

Single crystal diamond and perfect graphite are each characterized by a single Raman line which appears at 1332 and 1580 cm^{-1}, respectively. Figures 11(a) and 11(b) show a micro-Raman spectrum of irradiated and unirradiated regions, respectively. It is seen that under respective laser parameters, the graphite peaks in Fig. 11(a) are absent and the diamond retains its original diamond composition as illustrated in Fig. 11(b). It should be noted that the micro-Raman measurement in Fig. 11(a) has been carried out after the removal of debris and traces in the focus of the laser beam. The reduced Raman intensities in the irradiated regions

#126118 - $15.00 USD Received 29 Mar 2010; revised 28 May 2010; accepted 29 May 2010; published 3 Jun 2010

are due to scattering by the periodic ripples formed in such a modified surface. This result is important for applications such as industrial research and analysis of the femtosecond ablation involving diamond.

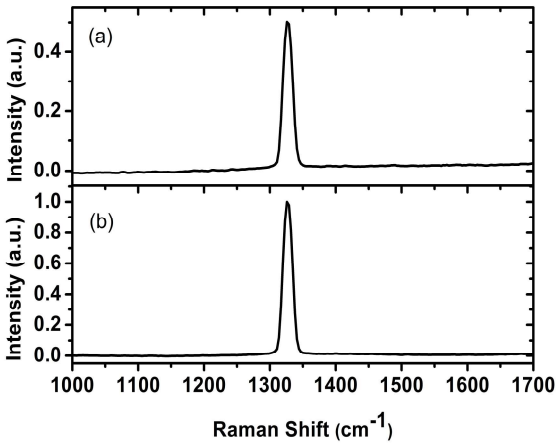

Fig. 11. (a) Micro-Raman spectrum of an irradiated area after debris removal and removal of any possible graphitized traces in the focus of the laser beam, and (b) Micro-Raman spectrum of an unirradiated area of a laser-processed synthetic single-crystal diamond sample. The irradiated region is shown in Fig. 10(b). The micro-Raman measurements were carried out using a 60X microscope objective with a numerical aperture of 0.85 using a 3 mW excitation power.

4. Summary

In conclusion, we demonstrated the fabrication of diversiform structures on HPHT synthetic single-crystal diamond by femtosecond laser irradiation using a newly developed scanning microscope. Design improvements suggest that a higher resolution pattern will have smoother features and that the overextension of the ablated region should be taken into account during the pattern designing process. An analysis of the variance of feature dimensions with increasing pulse energy reveals that the sample's unablated surface at the feature boundary to recede. The measured dimensions exhibited in this work almost linearly increase with greater laser pulse energy for this material. Overall, the most accurate and precise emulation of design is obtained when ablating with relatively low energy. Also, we have used Raman spectroscopy to show that under respective laser parameters and post-ablation cleaning strategy, the graphite peaks are absent and the diamond structures retain the original diamond composition.

Using pulse energies that are significantly above the threshold for permanent change, it is shown from this work that femtosecond laser machining provided negligible collateral heating and shock-wave damage. This is attributed to the low thermal losses and negligible hydrodynamic expansion of the ablated material during the femtosecond laser pulse. The upper limits on laser pulse energy, number of pulses and number of passes used in this study are 2.52 μJ, 750 and 3 respectively.

Although the number of incident pulses controls the feature size, the spontaneous formation of the periodic ripples on the surface of synthetic single-crystal diamond sample after irradiation with either single-pulse per site or at 250 kHz repetition rate (750 overlapping pulses) showed similar patterns at relatively low laser pulse energies. These phenomena require further investigations.

These results provide openings to further research in femtosecond laser micro-fabrication in wide bandgap materials, and are of prime interest for potential applications in controlled nanonstructuring, as well as various biotechnology related applications. With a basic knowledge of the ablation process and its important parameters and enhancement options, micro-/nano-structuring with femtosecond pulses can be continuously improved.

#126118 - $15.00 USD Received 29 Mar 2010; revised 28 May 2010; accepted 29 May 2010; published 3 Jun 2010

Acknowledgments

The synthetic single crystal diamond samples were furnished by Tom Smith, President of Diamond Edge Company. The authors acknowledge funding from the Tennessee Higher Education Commission through the Center for Laser Applications at University of Tennessee Space Institute. Ms. Intesar Zalloum helped in the editing and the graphics of the manuscript. Finally, we are indebted to three unknown referees for their advice and critical review of the manuscript.

#126118 - $15.00 USD Received 29 Mar 2010; revised 28 May 2010; accepted 29 May 2010; published 3 Jun 2010